IOPscience iopscience.iop.org

Home Search Collections Journals About Contact us My IOPscience

Interference in electron Compton scattering for silicon

This article has been downloaded from IOPscience. Please scroll down to see the full text article.

1996 J. Phys.: Condens. Matter 8 2835

(http://iopscience.iop.org/0953-8984/8/16/013)

View the table of contents for this issue, or go to the journal homepage for more

Download details:
IP Address: 171.66.16.208
The article was downloaded on 13/05/2010 at 16:33

Please note that terms and conditions apply.

J. Phys.: Condens. Matter **8** (1996) 2835–2850. Printed in the UK

Interference in electron Compton scattering for silicon

A Exner†, H Kohl‡, M Nelhiebel and P Schattschneider

Institut für Angewandte und Technische Physik, Wiedner Hauptstraße 8-10, A-1040 Wien, Austria

Received 3 July 1995, in final form 21 September 1995

Abstract. Starting from an expression for the double-differential cross section for electron Compton scattering in a crystal for a two-beam case, valid for a small Ewald sphere, the contributions of M-shell and L-shell electrons in silicon to the mixed dynamic form factors are calculated. The shape and intensity of the interference effects that superimpose on the Compton profile are determined. It is shown that the appearance of interference terms renders the cross section asymmetric and dependent on the momentum transfer also in the usual momentum representation. A procedure for an experimental investigation of the interference terms is proposed.

1. Introduction

In a Compton scattering experiment a probe particle, photon or electron, with momentum $\hbar\boldsymbol{p}_0$ and energy E_0 hits a target electron with momentum $\hbar\boldsymbol{p}$ and is detected with the energy $E_0 - \Delta E$ and change of momentum $\hbar\boldsymbol{q}$. Using the equations of energy and momentum conservation yields, for electrons as probes,

$$\Delta E = \frac{\hbar^2}{2m_e}(q^2 + 2\boldsymbol{q}\cdot\boldsymbol{p}) \tag{1}$$

where the first contribution to the energy loss is due to the loss of momentum of the probe in the scattering and the second contribution is a Doppler shift due to the motion of the target before the scattering event. Thus, the energy loss is proportional to the projection of the target momentum onto the direction of the momentum-transfer vector. So, the Compton scattering distribution for fixed $\boldsymbol{q}$ as a function of ΔE monitors the momentum distribution of the target, projected onto $\boldsymbol{q}$.

In a crystal, however, the momentum operator does not commute with the crystal Hamiltonian, which excludes states being both momentum eigenstates and stationary. So, the probe momentum before and after the scattering in the crystal is unknown, and (1) is no longer valid. The incoming plane wave describing the probe electron in vacuum has to be expanded as a sum of Bloch waves, the stationary electron states in the crystal potential. For the scattered electron, we will neglect the influence of the crystal potential, here. Under the experimental conditions to be discussed, it can be described by a plane wave. The fact that the wave function of the incoming probe electron has to be written as a sum over Bloch

† Now at: Institut für Strömungslehre und Wärmeübertragung, Wiedner Hauptstraße 7, A-1040 Wien, Austria.
‡ Westfälische Wilhelms-Universität Münster, Physikalisches Institut, Wilhelm-Klemm-Straße, 10, D-48149 Münster, Germany.

0953-8984/96/162835+16$19.50 © 1996 IOP Publishing Ltd

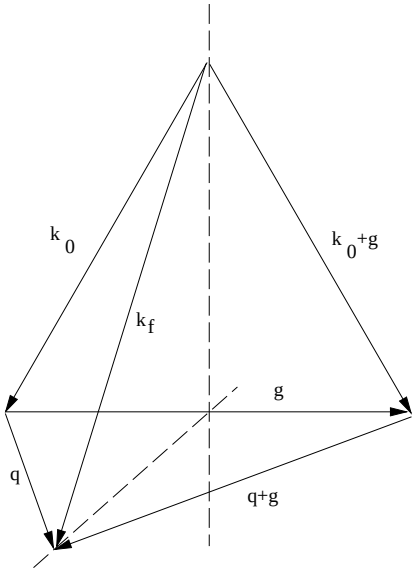

Figure 1. Bloch wave vectors and momentum transfer in a symmetric two-beam case.

waves leads to the appearance of interference terms in the result. This modifies the form of the double-differential cross section.

The expression for the double-differential cross section for inelastic electron scattering in a crystal has been derived in a previous paper henceforth referred to as paper I (Exner *et al* 1994). We will only give the result here. The double-differential cross section was obtained on the assumption that the incoming probe electron, being in a plane-wave state in vacuum, splits into a sum of Bloch waves in the crystal. In a two-beam case (Jonas and Schattschneider 1993), the incoming electron with momentum $\hbar\boldsymbol{k}_i$ is described by a sum of two Bloch waves (Reimer 1984) with Bloch wave vectors $\boldsymbol{k}_i$ and $\boldsymbol{k}_i + \boldsymbol{g}$ with a reciprocal-lattice vector $\boldsymbol{g}$ which is the Bragg vector of the two-beam case. After the scattering, the probe electron is detected in a plane-wave state with momentum $\hbar\boldsymbol{k}_f$ (figure 1). Here, we have made the approximation of a small Ewald sphere. In the case where this approximation is not fulfilled the probe electron state in the crystal after the scattering is also a sum over Bloch waves and the expression for the cross section becomes more complicated. This case will not be part of this paper.

The calculation has been made using the impulse approximation (Eisenberger and Platzman 1970, Schattschneider *et al* 1990), i.e. the energy loss of the probe substantially exceeds the binding energy of the target electron.

In paper I, the interference term of 3s electrons was calculated analytically. It was shown that this term is negligible for sufficiently high $|\boldsymbol{g}|$. Here, we extend the calculations to silicon p states and to L-shell electrons. We start from the expression for the cross section $\partial^2\sigma/\partial\Omega\,\partial E$—equation (8) in paper I—and discuss both the direct and indirect terms for L- and M-shell electrons. The K-shell electrons will not be treated in the calculation since their ionization energy lies at 1840 eV whereas the typical energy losses in electron Compton scattering are 1000–1300 eV. An experiment is proposed in which the indirect terms could be measured. It is shown that the L-shell electrons contribute considerably to the indirect term, in a way that masks the effect of the valence electrons.

2. The double-differential cross section

The double-differential cross section for electron scattering in the two-beam case for the conditions described above is (see equation (8) in paper I)

$$\frac{\partial^2\sigma}{\partial E\,\partial\Omega} \propto S_{At}(\boldsymbol{q},\boldsymbol{q},E) - \frac{K_g}{K_0}\frac{w}{1+w^2}\left(1-\frac{\sin\delta}{\delta}\right)S_{At}(\boldsymbol{q},\boldsymbol{q}+\boldsymbol{g},E) \tag{2}$$

with the vector of momentum transfer $\hbar\boldsymbol{q} = \hbar(\boldsymbol{k}_i - \boldsymbol{k}_f)$ and the energy loss of the probe electron $E = \hbar\omega$. The geometry of the experiment is chosen such that $q = |\boldsymbol{q}+\boldsymbol{g}|$. Taking account of the crystal symmetry, this implies that $S_{At}(\boldsymbol{q},\boldsymbol{q},\omega) = S_{At}(\boldsymbol{q}+\boldsymbol{g},\boldsymbol{q}+\boldsymbol{g},\omega)$. w is the excitation error in units of the extinction distance ξ_g (Reimer 1984). δ is given as $\delta = d(\gamma^{(1)} - \gamma^{(2)})$ with the specimen thickness d and the *anpassungen* (Reimer 1984)

$$\gamma^{(i)} = \frac{\pi}{\xi_g}\left[w - (-1)^i\sqrt{1+w^2}\right].$$

The difference $\gamma^{(1)} - \gamma^{(2)}$ is the separation of the dispersion surfaces of the probe electron in the crystal. The structure factor K_g for silicon in a centrosymmetric description is $K_g = 2\cos\left[(\pi/4)(h+k+l)\right]$ where (hkl) are the Miller indices of the reciprocal-lattice vector $\boldsymbol{g}$. The mixed dynamic form factor (MDFF) $S_{At}(\boldsymbol{q},\boldsymbol{q}',\omega)$ is defined as

$$S_{At}(\boldsymbol{q},\boldsymbol{q}',\omega) = \sum_\nu \int \mathrm{d}^3p\ \tilde\varphi_\nu^*(\boldsymbol{p}-\boldsymbol{q})\tilde\varphi_\nu(\boldsymbol{p}-\boldsymbol{q}')\,\delta\left\{\omega - \frac{\hbar}{2m}\left[\boldsymbol{p}(\boldsymbol{q}+\boldsymbol{q}') - \frac{q^2+q'^2}{2}\right]\right\} \tag{3}$$

where $\tilde\varphi_\nu(\boldsymbol{p})$ are atomic orbitals in the momentum representation and the sum is over all occupied states. ν stands for the set of atomic quantum numbers (n,l,μ). The subscript 'At' denotes that (3) contains the atomic contribution to the scattering cross section (2). The cross section (2) consists of a linear combination of two† MDFF. The first one is a direct term, i.e. identical to the ordinary atomic structure factor $S(q,E)$. The second, indirect term is a consequence of interference between the two incident beams, set up by diffraction in the crystal. The prefactor depends on the crystal orientation.

In the following, we will show how the MDFF can be calculated for analytically given wave functions for silicon. For $\boldsymbol{q} = \boldsymbol{q}'$ we call $S_{At}(\boldsymbol{q},\boldsymbol{q}',\omega)$ the direct MDFF; for $\boldsymbol{q} \neq \boldsymbol{q}'$ we call it the indirect MDFF. The MDFF were calculated from wave functions which have been taken from a work of Duncanson and Coulson (1947). For the L shell ($n = 2$) and M shell ($n = 3$) in reciprocal space they have the form

$$\begin{aligned}
\varphi_{200}(\boldsymbol{p}) &= \sqrt{\frac{2c_{20}^5}{3\pi^2}}\frac{(6c_{20}^2 - 2p^2)}{(c_{20}^2+p^2)^3}\\
\varphi_{21\mu}(\boldsymbol{p}) &= \sqrt{\frac{8c_{21}^5}{3\pi}}\frac{8c_{21}p}{(c_{21}^2+p^2)^3}P_\mu(\vartheta,\varphi)\\
\varphi_{300}(\boldsymbol{p}) &= \sqrt{\frac{4c_{30}^7}{45\pi^2}}24c_{30}\frac{(c_{30}^2-p^2)}{(c_{30}^2+p^2)^4}\\
\varphi_{31\mu}(\boldsymbol{p}) &= \sqrt{\frac{16c_{31}^7}{45\pi}}8p\frac{(5c_{31}^2-p^2)}{(c_{31}^2+p^2)^4}P_\mu(\vartheta,\varphi)
\end{aligned} \tag{4}$$

† Originally, there are three terms, namely including a second direct term $S_{At}(\boldsymbol{q}+\boldsymbol{g},\boldsymbol{q}+\boldsymbol{g},\omega)$, which was set equal to the first direct term for reasons explained above. Those two terms are also expected in the kinematic case, i.e. when two beams are incident in directions **0** and $\boldsymbol{g}$.

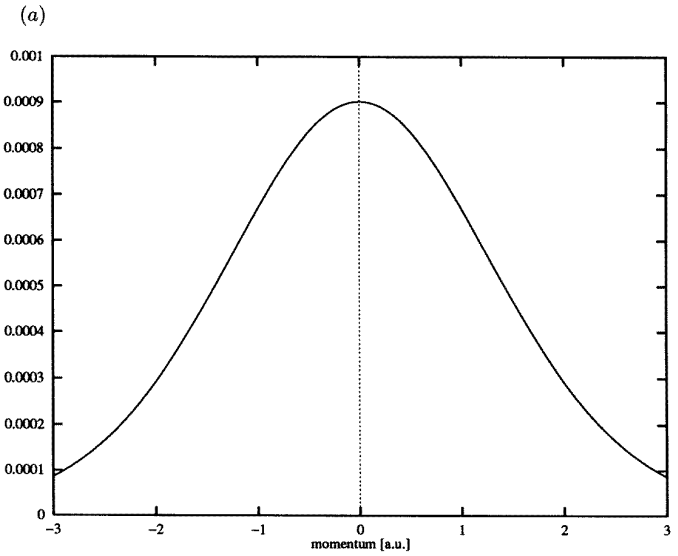

(a)

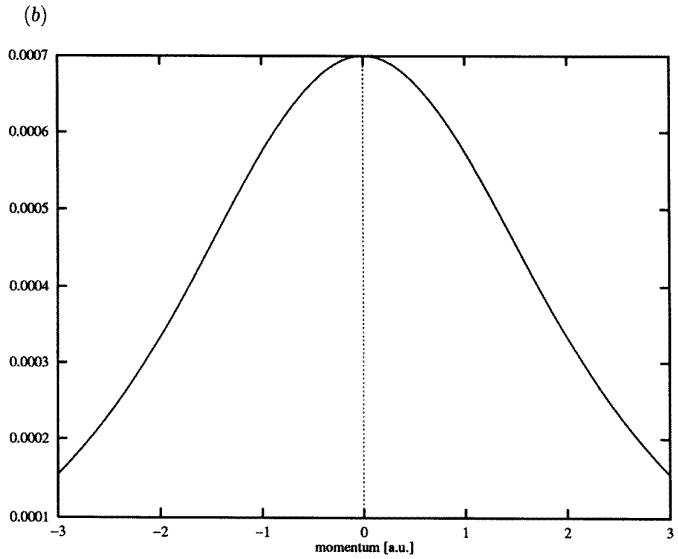

(b)

Figure 2. Contributions to the direct MDFF $\times 10^{15}$ of the L-shell electrons with $l = 0$ (a) and $l = 1$, $\mu = x$ (b), $\mu = y$ (c), and $\mu = z$ (d), and of the M-shell electrons with $l = 0$ (e) and $l = 1$, $\mu = x$ (f), $\mu = y$ (g), and $\mu = z$ (h).

where the quantum number μ stands for directions of the angular momentum (x, y, z) and the real-valued combinations $P_{x_i}(\Omega)$ of the spherical harmonics $Y_1^1(\Omega)$, $Y_1^0(\Omega)$, $Y_1^{-1}(\Omega)$ are given by

$$P_x(\vartheta, \varphi) = \sin\vartheta \cos\varphi$$

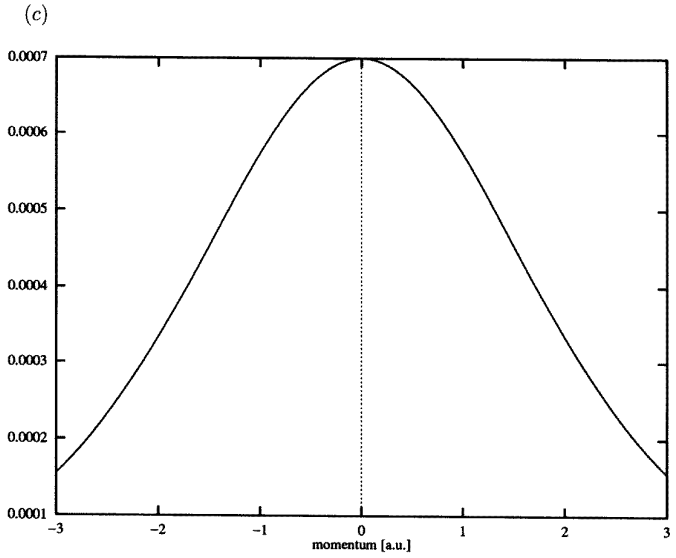

(c)

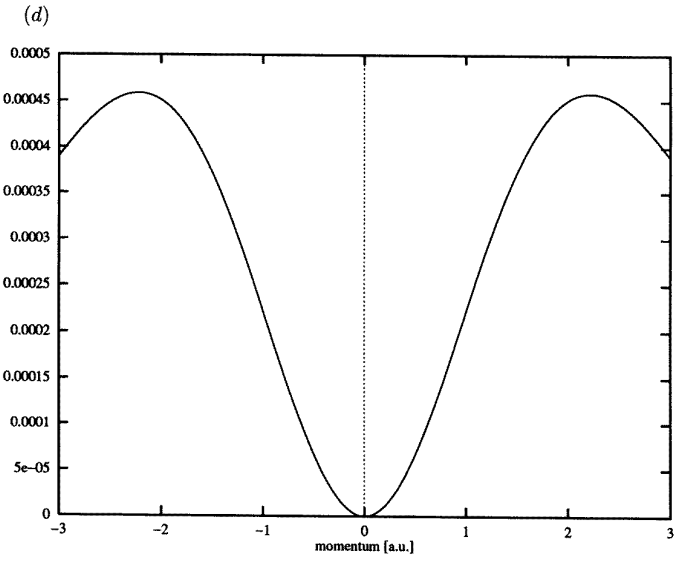

(d)

Figure 2. (Continued)

$$P_y(\vartheta, \varphi) = \sin\vartheta \sin\varphi \qquad (5)$$
$$P_z(\vartheta, \varphi) = \cos\vartheta.$$

Note that μ should not be mixed up with the usual magnetic quantum number m.

The parameters c_{nl} depend on the screening constant σ_{nl} via the relation $c_{nl} = (Z - \sigma_{nl})/n$ with the atomic number Z ($Z = 14$ for silicon). The values for c_{nl} were obtained by comparing the Compton profiles of the orbitals (4) to the Compton profiles

(*e*)

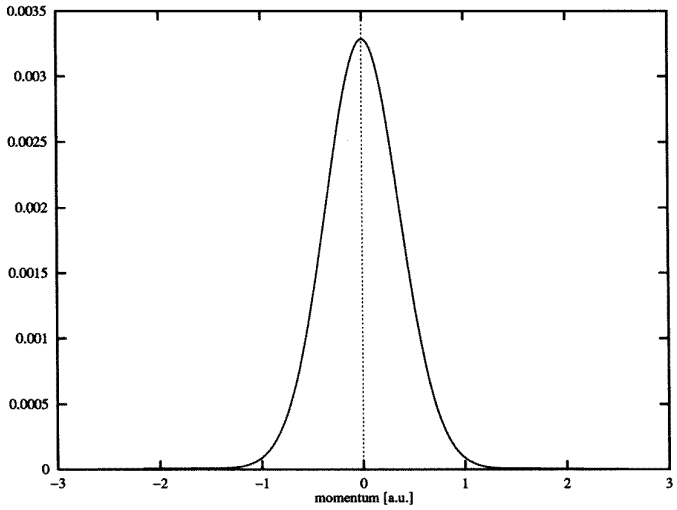

(e)

(*f*)

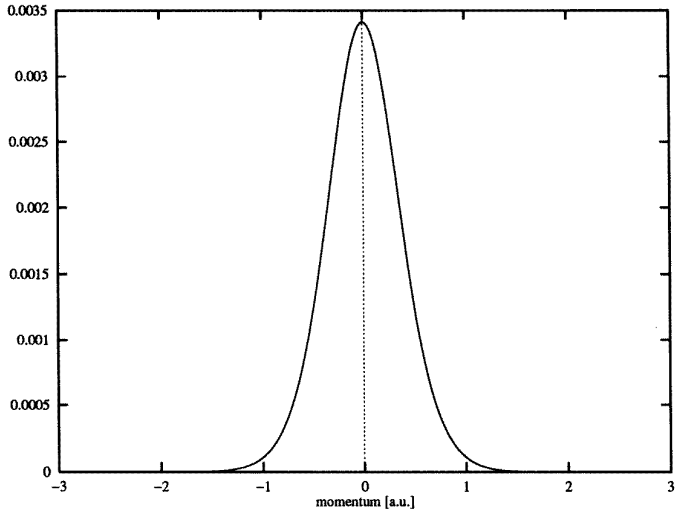

(f)

Figure 2. (Continued)

calculated by Biggs *et al* (1975) for Hartree–Fock wave functions. The parameters and corresponding screening constants are given in table 1.

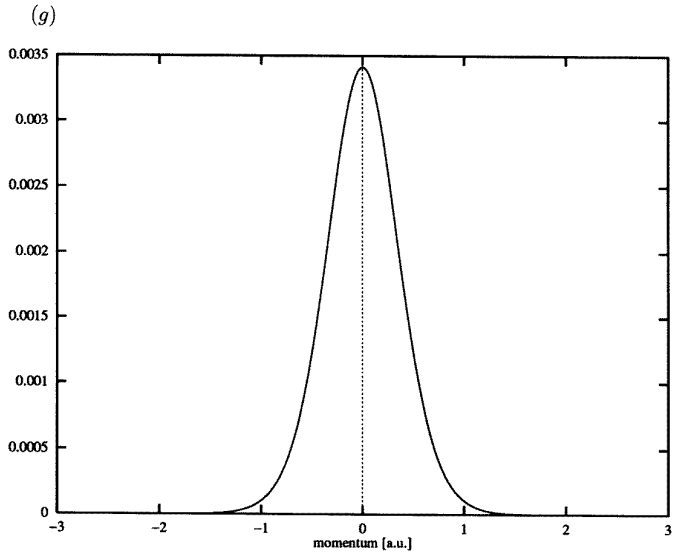

(g)

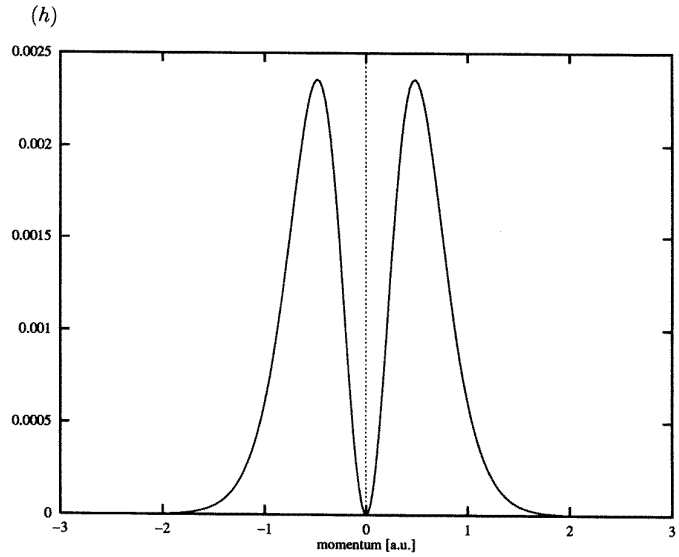

(h)

Figure 2. (Continued)

3. Direct and indirect mixed dynamic form factors

The direct MDFF can be calculated analytically from (3) for the wave functions (4) by performing elementary integrations. We will give only the main features of the calculation and discuss the physical contents of the MDFF.

Table 1. c_{nl} in atomic units and related screening constants σ_{nl}.

n	c_{n0}	c_{n1}	σ_{n0}	σ_{n1}
2	4.40	4.45	5.20	5.10
3	1.58	1.23	9.25	10.31

We set $\boldsymbol{q} = \boldsymbol{q}'$ in (3), transform the coordinates using $\boldsymbol{\xi} = \boldsymbol{p} - \boldsymbol{q}$, and get

$$S_{At}(\boldsymbol{q}, \boldsymbol{q}, \omega) = \frac{m}{\hbar q} \sum_{\nu} \int \mathrm{d}^3\xi \ |\tilde{\varphi}_\nu(\boldsymbol{\xi})|^2 \, \delta(\xi_z - \xi_{z0}^{(d)})$$
$$\hbar\xi_{z0}^{(d)} := \frac{m}{\hbar q}\left(\hbar\omega - \frac{\hbar^2 q^2}{2m}\right) \tag{6}$$

where we have chosen the z-axis parallel to $\boldsymbol{q}$. The expression in parentheses in the definition of the momentum z-coordinate $\hbar\xi_{z0}^{(d)}$ is the difference between the energy loss of the probe electron and the kinetic energy the target electron would have acquired if it were at rest before the scattering event. The index (d) indicates that $\xi_{z0}^{(d)}$ is a parameter appearing in the direct MDFF. The integral in (6) is the contribution of the orbital with the quantum numbers ν to the Compton profile (Jonas and Schattschneider 1993) and the energy of the Compton maximum is defined by $\xi_{z0}^{(d)}(\omega_{max}, q) = 0$, i.e. $\hbar\omega_{max} = \hbar^2 q^2/2m$. Since the $\tilde{\varphi}_\nu(\boldsymbol{p})$ that we used are either symmetric or antisymmetric functions of any of their Cartesian coordinates (p_x, p_y, p_z) the square is symmetric with respect to $\xi_z = 0$, and the MDFF which is a function of $\xi_{z0}^{(d)}(\omega, q)$ is symmetric with respect to the Compton maximum $\xi_{z0}^{(d)} = 0$ as it has to be for a Compton profile.

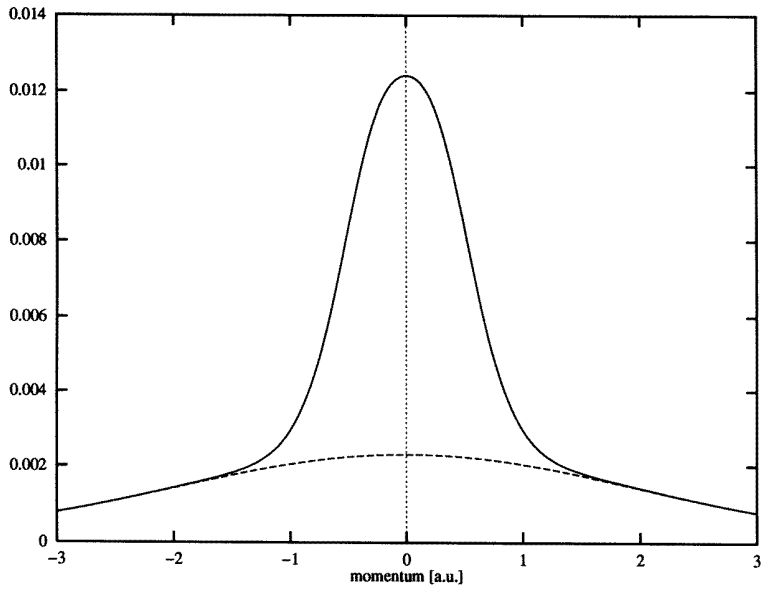

Figure 3. The direct MDFF $\times 10^{15}$ or the Compton profile. The dashed curve shows the contribution of L-shell electrons.

In figure 2 the contributions of the occupied L-shell and M-shell electron states in silicon

to the MDFF are given in a momentum representation. Figure 3 shows the Compton profile (6) with the contribution of all L-shell electrons given as a dashed curve.

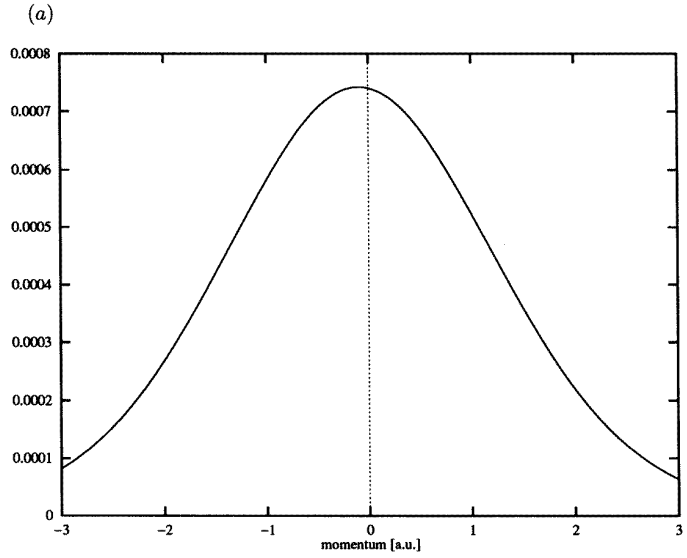

(a)

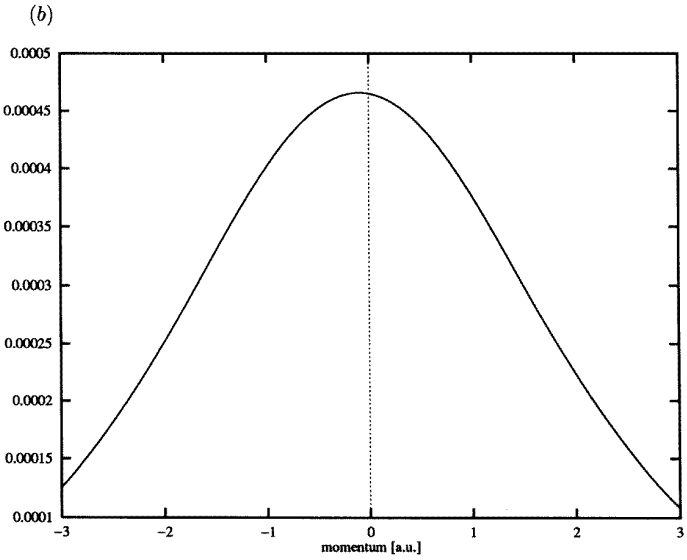

(b)

Figure 4. Contributions to the indirect MDFF $\times 10^{15}$ for $q = 150$ nm^{-1} and $\boldsymbol{g} = (220)$ of the L-shell electrons with $l = 0$ (a) and $l = 1$, $\mu = x$ (b), $\mu = y$ (c), and $\mu = z$ (d), and of the M-shell electrons with $l = 0$ (e) and $l = 1$, $\mu = x$ (f), $\mu = y$ (g), and $\mu = z$ (h).

For the indirect MDFF, the change of coordinates and the transformation of the δ-

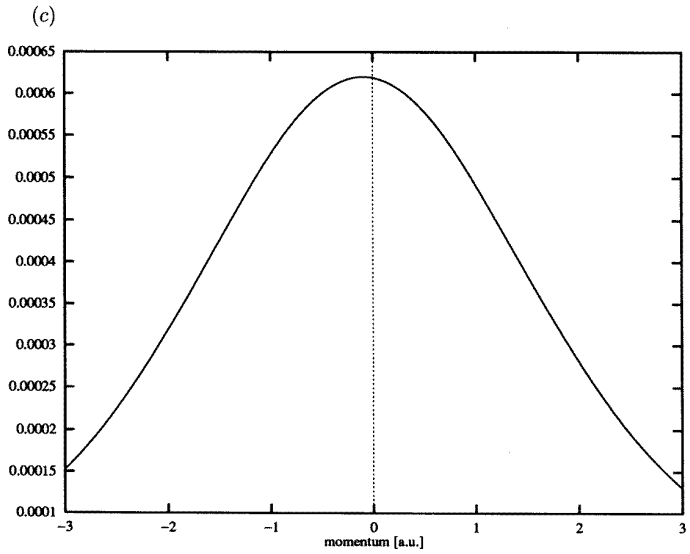

(c)

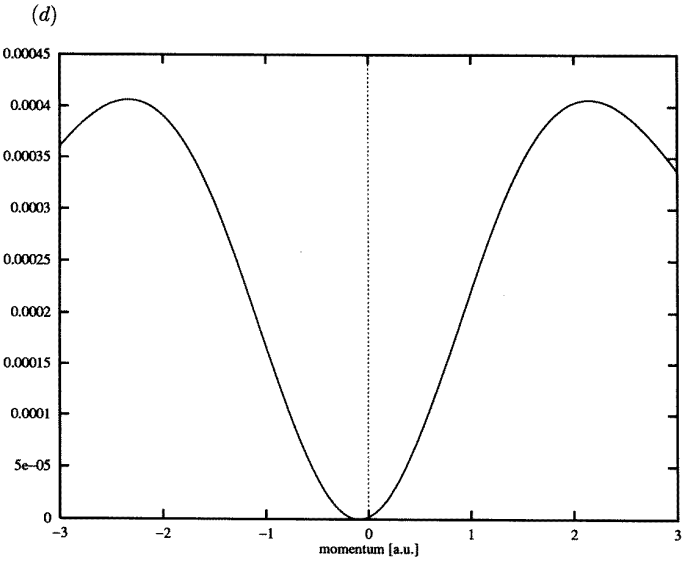

(d)

Figure 4. (Continued)

function lead to

$$S_{At}(\boldsymbol{q},\boldsymbol{q}',\omega)=\frac{2m}{\overline{h}|\boldsymbol{q}+\boldsymbol{q}'|}\sum_{\nu}\int \mathrm{d}^3\xi\ \tilde{\varphi}^*_{\nu}(\boldsymbol{\xi})\tilde{\varphi}_{\nu}(\boldsymbol{\xi}+\boldsymbol{g})\ \delta(\xi_z-\xi^{(i)}_{z0})$$
$$\overline{h}\xi^{(i)}_{z0}:=\frac{2m}{\overline{h}|\boldsymbol{q}+\boldsymbol{q}'|}\left(\overline{h}\omega-\frac{\overline{h}^2q^2}{2m}-\frac{\overline{h}^2\boldsymbol{q}\cdot\boldsymbol{g}}{2m}\right). \tag{7}$$

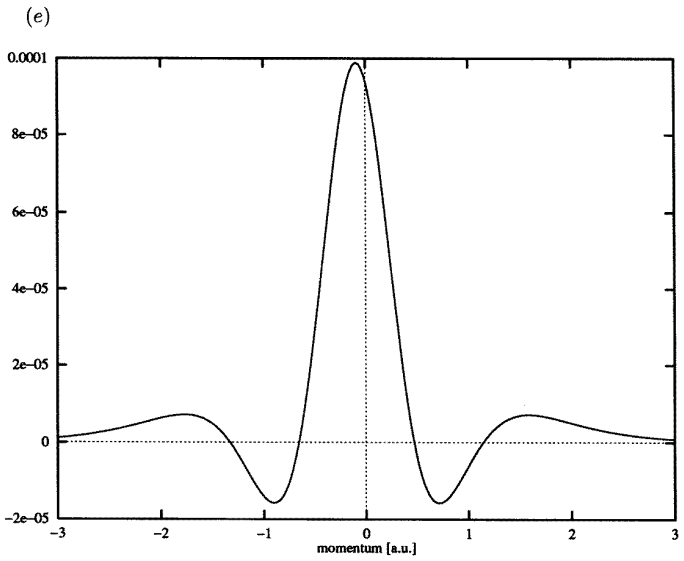

(e)

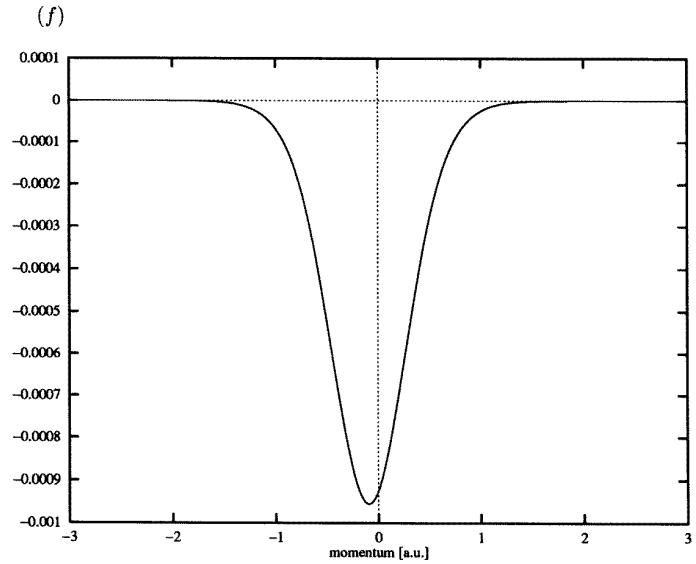

(f)

Figure 4. (Continued)

Since we are discussing the case where $q = |\boldsymbol{q} \cdot \boldsymbol{g}|$, $\xi_{z0}^{(i)}$ can be written as (see figure 1)

$$\hbar\xi_{z0}^{(i)} = \frac{2m}{\hbar|\boldsymbol{q}+\boldsymbol{q}'|}\left(\hbar\omega - \frac{\hbar^2 q^2}{2m} + \frac{\hbar^2 g^2}{4m}\right). \tag{8}$$

By comparison with $\xi_{z0}^{(d)}$ (equation (6)) we find that the energy $\hbar\omega_0$ with $\xi_{z0}^{(i)}(\omega_0) = 0$ is

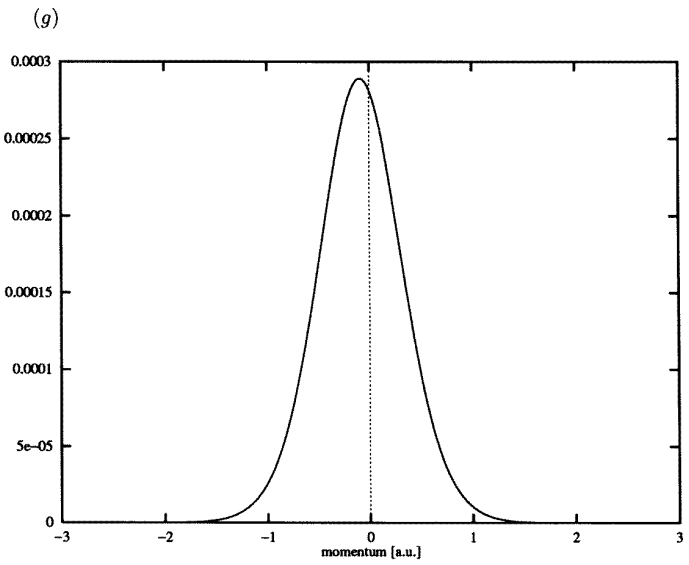

(g)

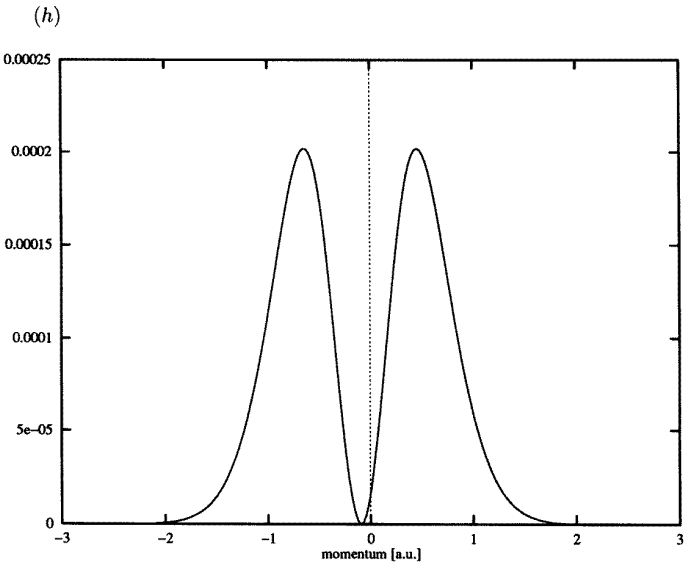

(h)

Figure 4. (Continued)

shifted† from the Compton maximum $\xi_{z0}^{(d)} = 0$ towards lower energies by $\hbar^2 g^2/4m$. This shift depends only on the Bragg vector $\boldsymbol{g}$ that causes the interference term and not on the momentum transfer. As can be seen from figure 4, $\xi_{z0}^{(i)} = 0$ is also a point of symmetry. This may equally be deduced from (4).

† This energy shift, although not visible at first glance, also appears in the nondiagonal Compton profiles given by Schülke and Mourikis (1986).

The additional energy shift of the indirect MDFF has two important consequences for the double-differential cross section. Firstly, since the cross section consists of a weighted sum of two symmetric functions each with a single point of symmetry, shifted against each other, the result is no longer symmetric with respect to any energy value. Secondly, the additional energy shift of the indirect MDFF is independent of the momentum transfer $\hbar\boldsymbol{q}$ and is constant for a given $\boldsymbol{g}$. This means that the cross section, measured for different $\boldsymbol{q}$ as a function of energy loss, is no longer independent of q when represented as a function of

$$\hbar\xi_{z0}^{(d)} = \frac{m}{\hbar q}\left(\hbar\omega - \frac{\hbar^2 q^2}{2m}\right)$$

i.e. of target momentum.

The contributions of the atomic orbitals to the indirect MDFF have been calculated numerically using a Simpson algorithm (Press *et al* 1986)†. They are given for three different Bragg vectors (220), (440), and (660) in figure 4. The x-axis was chosen to be parallel to $\boldsymbol{g}$. The main features of the results can be explained by the fact that the indirect MDFF are overlap integrals of a wave function centred at $\boldsymbol{\xi}$ with the same wave function centred at $\boldsymbol{\xi} + \boldsymbol{g}$. The bigger g, the smaller the overlap, and the results show that the intensity of the MDFF decreases with increasing Bragg vector. Since the L-shell electrons are more strongly localized in space than the M-shell electrons, the L-shell wave functions are broader in reciprocal space and so the overlap is stronger for L-shell electrons. All orbitals with $m = z$ vanish in the plane $\xi_z = 0$, i.e. for $\xi_{z0} = 0$ the contribution to the MDFF has a minimum with value 0. The additional energy shift for the indirect MDFF can be excellently observed in the position of this point, which is drifting to the left with increasing g. The indirect MDFF, unlike the direct MDFF, can have negative intensity, which for $m = x$ is caused by the angular part of the wave functions‡ and for $l = 0$ or $n = 3$ by a change in sign of the radial parts§. The momentum for which this change in sign occurs depends on the parameters c_{nl} and therefore on the effective nuclear charge that the electron with quantum numbers n, l sees.

The results of the present numerical integration coincide excellently with the analytical results obtained in paper I. Differences between the analytically and numerically calculated functions could not be detected within the accuracy of our calculations. The indirect MDFF that are obtained by adding the contributions of all of the orbitals are displayed in figure 5, (a)–(c). The contribution of all of the L-shell electrons is shown as a dashed curve.

4. The influence of the indirect MDFF

For $q = |\boldsymbol{q} + \boldsymbol{g}|$, the double-differential cross section simplifies to the expression given in (2). It is the sum of the Compton profile $S_{At}(\boldsymbol{q}, \boldsymbol{q}, \omega)$ and the product of the interference term with a function which depends on the excitation error w and via δ on the specimen thickness d. For specimen thicknesses $d = 0.5\xi_g$ and $d = 0.7\xi_g$ this function is shown in figure 6. From (2) and figure 6 one can see how the indirect MDFF can be made visible in the experiment. If the double-differential cross section is measured for two different excitation errors w_1 and w_2, preferably with opposite sign, then the indirect MDFF can be extracted from the experimental data by simply subtracting the two spectra from each other.

† The MDFF can be calculated for all Bragg vectors for silicon. The computer program is available on request.

‡ Though for the L shell and small g this effect is compensated by the radial parts.

§ Compare also the change in sign of the indirect MDFF for 3s electrons in paper I for growing $\boldsymbol{g}$.

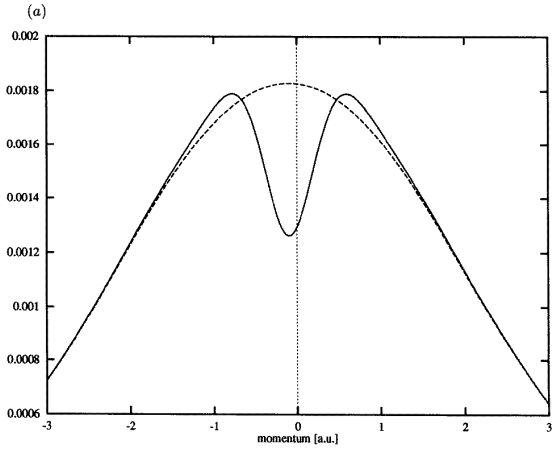

(a)

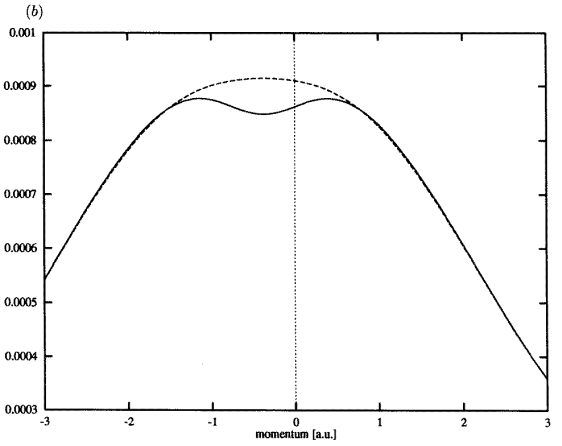

(b)

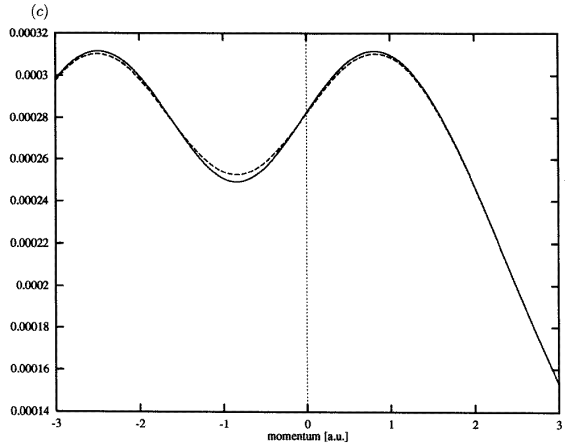

(c)

Figure 5. The indirect MDFF $\times 10^{15}$ for $q = 150$ nm^{-1} and $\boldsymbol{g} = (220)$ (a), $\boldsymbol{g} = (440)$ (b), and $\boldsymbol{g} = (660)$ (c). The contribution of the L-shell electrons alone is shown as a dashed line.

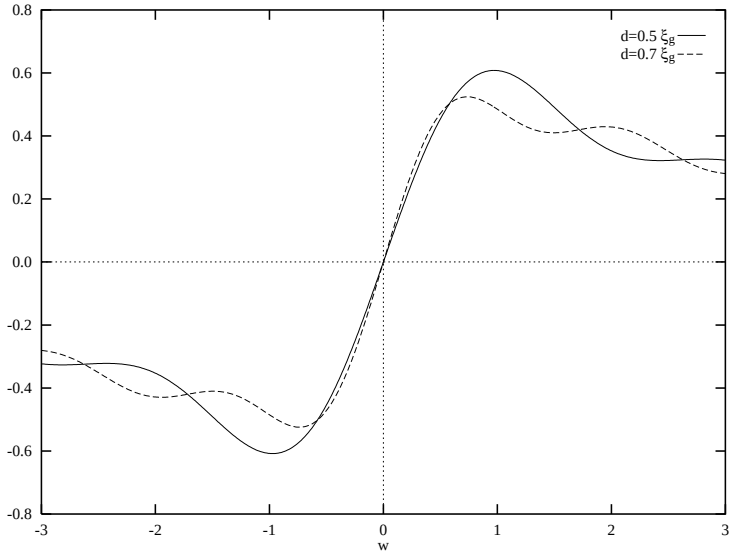

Figure 6. The w-dependence of the interference contribution to the double-differential cross section for specimen thicknesses $d = 0.5\xi_g$ and $d = 0.7\xi_g$.

The relative intensity of the result compared to the direct MDFF depends on the w chosen, on the specimen thickness and on the Bragg vector of the two-beam case.

The indirect MDFF was measured in an ingenious Compton scattering experiment (Schülke and Mourikis 1986) and recently with synchrotron radiation (Spiertz *et al* 1994). The equations are more complicated in the photon case, due to polarization; unlike for electron Compton scattering, macroscopic specimens are needed.

The maximal difference is reached for $w_{1,2} = \pm 1$ and

$$\frac{d}{\xi_g} = \frac{1}{\sqrt{2}\pi} \tan\left(\pi\sqrt{2}\frac{d}{\xi_g}\right).$$

An approximate solution for the second condition is

$$\frac{d}{\xi_g} = \frac{2n-1}{2\sqrt{2}} \qquad n \in \mathbb{N}.$$

For $w_1 = 1$, $w_2 = -1$ and $d = \xi_g$ the difference of the two spectra (2) gives $1.2(K_g/K_0)S_{At}(\boldsymbol{q}, \boldsymbol{q}+\boldsymbol{g}, \omega)$. The intensity of the strongest indirect MDFF given above, $\boldsymbol{g} = (220)$, is about >10% of the intensity of the direct MDFF. This effect comes mainly from the L-shell electrons. Often, though, one is interested only in the contribution of the valence electrons. In this case, the maximal effect is only about 6%. The effect is strongly decreasing with increasing g.

5. Conclusions

Interference effects have a significant influence on Compton scattering in a crystal when low-indexed Bragg reflexes are involved. The interference terms in the double-differential cross section can be interpreted as overlap integrals of the atomic orbitals in reciprocal space. The stronger effects come from the inner-shell electrons because of their stronger localization in space. The shape of the cross section, though, is more strongly influenced

by the interference terms of the valence electrons. An additional energy shift of the point of symmetry of the interference terms with respect to the Compton maximum breaks the symmetry of the cross section. It should be mentioned once more that the above calculations were made on the assumption of a small Ewald sphere. For the more general case, the interference effects become stronger and more complicated. We have also investigated this case and it will be the subject of a forthcoming paper.

Acknowledgment

We thank the Hochschuljubiläumsstiftung der Stadt Wien for financial support.

References

Biggs F, Mendelsohn M B and Mann J B 1975 *At. Data Nucl. Data Tables* **16** 201
Duncanson W E and Coulson C A 1947 *Proc. Phys. Soc.* **LX2** 175
Eisenberger P and Platzman P M 1970 *Phys. Rev.* A **2** 415
Exner A, Kohl H, Schattschneider P and Jonas P 1994 *J. Phys.: Condens. Matter* **6** 3443
Jonas P and Schattschneider P 1993 *J. Phys.: Condens. Matter* **5** 7173
Press W H, Fannery B P, Teukolsky S A and Vetterling W T 1986 *Numerical Recipes* (Cambridge: Cambridge University Press)
Reimer L 1984 *Transmission Electron Microscopy* (Berlin: Springer)
Schattschneider P, Pongratz P and Hohenegger P 1990 *Scanning Microsc. Suppl.* **4** 35
Schülke W and Mourikis S 1986 *Acta Crystallogr.* A **42** 86
Spiertz A, Höppner K, Gabriel K, Kaprolat A and Schülke W 1994 *Sagamore XI (Brest)* ed G Loupias and S Rabii; Université Pierre et Marie Curie, extended abstracts, p 107